SnP nanocrystals as anode material for Na-ion battery

Junfeng Liu[†], Shutao Wang[‡§], Kostiantyn Kravchyk[‡§], Maria Ibáñez[‡§], Déspina Nasiou[∇], Michaela Meyns[*†], Jordi Llorca[⊥], Jordi Arbiol[∇#], Maksym V. Kovalenko[‡§], and Andreu Cabot[*†#]

[†] Catalonia Institute for Energy Research − IREC, 08930 Sant Adrià de Besòs, Barcelona, Spain

[‡] Institute of Inorganic Chemistry, Department of Chemistry and Applied Biosciences, ETH Zürich, Zürich, CH-8093,Switzerland

[§] EMPA-Swiss Federal Laboratories for Materials Science and Technology, Dübendorf, CH-8600, Switzerland

[∇] Catalan Institute of Nanoscience and Nanotechnology- ICN2, CSIC and BIST, Campus UAB, 08193 Barcelona, Spain

[⊥] Institut de Tècniques Energètiques, Universitat Politècnica de Catalunya, 08028 Barcelona, Spain

[#] ICREA, Pg. Lluis Companys 23, 08010 Barcelona, Catalonia, Spain

Supporting Information Placeholder

ABSTRACT: We report the synthesis of SnP nanocrystals (NCs) from the reaction of hexamethylphosphorous triamide (HMPT) and a tin phosphonate prepared from tin oxalate and a phosphonic acid. SnP NCs displayed spherical geometry and a trigonal crystallographic phase with a superstructure attributed to ordered diphosphorous pairs. Sodium ion batteries (SIBs) based on SnP NCs and NaFSI electrolyte displayed high reversible capacities of 600 mA h g^{-1} at a current density of 100 mA g^{-1} and cycling stability for over 200 cycles.

Phosphorous, tin, antimony and alloys based on these elements are among the best candidate anode materials for SIBs.[1] In particular, elemental phosphorous has a very high theoretical capacity of 2596 mA h g^{-1} corresponding to the formation of Na_3P.[2] However, phosphorous has a limited electrical conductivity. Additionally, it displays a huge volumetric change, 490%, during formation of the Na-rich phase, which results in pulverization and peeling off from the current collector.

To overcome limitations of pure phosphorous, combinations of phosphorus with metals forming metal phosphides have been proposed. Among them, tin phosphides, with two electroactive elements, have certainly attracted much attention as low-cost anode material with high theoretical capacity, 1132 mAh g^{-1} for Sn_4P_3, associated with the formation of Na_3P and $Na_{15}Sn_4$.[3]

Besides a proper composition, to optimize performance and cycling stability, the use of nanostructured materials is crucial. Nanomaterials can reduce the accumulated stress during sodiation, enhance electron and ion transport when within a conductive matrix and improve the kinetics of sodium insertion/removal.[4]

Reliable strategies to produce metal phosphide NCs with controlled parameters are not yet well developed. Particularly challenging is the synthesis of phosphides of main group metals, including Sn.[5] In the past, various synthetic approaches of tin phosphides were developed, mostly resulting in Sn_4P_3. While demonstrating high capacity values and low redox potentials,[3b,c] Sn_4P_3 showed poor cycling performance. Alternative phosphorus-richer tin phosphides have higher theoretical mass capacities. However, due to the challenge that the synthesis of tin phosphide phases different from Sn_4P_3 has so far represented, just one phosphorus-rich tin phosphide, SnP_3, prepared by reactive ball milling of Sn, red phosphorous and carbon black, has been tested as anode material for SIBs.[3g]

A tin phosphide yet to be explored for a number of potential applications, including SIBs, is SnP. SnP is a metastable tin phosphide phase, but displaying a large kinetic stability at temperatures below 500 °C.[6] SnP has a layered structure composed of Sn-P-P-Sn sandwiches stacked together to form a three-dimensional crystal.[7] Its layered structure, metallic character and stoichiometric composition, with a theoretical capacity of 1209 mA h g^{-1}, make SnP an excellent candidate anode material for SIBs. Actually, the existence of diphosphorus pairs in the SnP structure has already been demonstrated to prevent phase segregation during lithiation/delithiation cycles,[8] resulting in a superior stability in LIB anodes.

In this work, we present a reliable synthetic approach to produce SnP NCs making use of stable and safe metal precursors. We further test the performance and stability of these SnP NCs as anode material for SIBs.

SnP NCs were prepared by reacting HMPT with a source of tin at 250-270 °C. The reaction was carried out

in an octadecene (ODE) solution containing tetradecylphosphonic acid (TDPA) and oleylamine (OAm), as detailed in the experimental section (SI). To optimize the synthetic procedure, different tin precursors were initially tested (SI). Among the different compounds tested, tin oxalate was the only one yielding pure phase SnP upon reaction with HMPT in the presence of a phosphonic acid and OAm. This experimental result and the advantageous stability, low cost and low toxicity of tin oxalate made us selecting this precursor as the most convenient one to continue this work.

To assess the role of TDPA, reactions with different amounts of this compound were carried out (Figure S4). In the absence of TDPA, tin oxalate did not fully dissolve in the ODE-OAm solution. Thus, upon injection of HMPT, Sn_4P_3 particles with a drop-like morphology and sizes above 200 nm mixed with small amounts of metallic Sn were produced (Figures S4a,e). Such morphology was similar to that obtained in a previous work from the reaction of tin(II) acetylacetonate with trioctylphosphine (TOP) at 350 °C.[3b] In this previous work, tin(II) acetylacetonate was found to decompose to SnO, which was reduced to Sn and later reacted with TOP to yield Sn_4P_3. In our reaction conditions, XRD and SEM-EDX analysis also demonstrated that in the absence of TDPA, tin oxalate initially decomposed to SnO, which later reacted with HMPT to yield Sn_4P_3 particles (Figures S5, S6).

With a TDPA/Sn ratio of 0.5, chains of aggregated NCs containing a blend of SnP and Sn phases were produced (Figure S4b). Phosphonic acids strongly coordinate to tin, helping to dissolve the tin oxalate in the ODE solution. However, with a low amount of TDPA, part of the oxalate was not dissolved, and a mixture of phases was still obtained. With a larger amount of TDPA, TDPA/Sn = 1, all the tin oxalate was well dissolved and a clear solution was obtained at 180 °C. After injecting HMPT, it took about 30 s for the color of the growth solution to change from colorless to black. The long nucleation time might be related to a strong binding of phosphonate to tin ions. Under these conditions, well-dispersed spherical 34 ± 5 nm NCs of pure SnP were obtained, and no extra phases were found from the XRD characterization (Figure 1a). The geometrical particle size matched well with the crystallographic size obtained from the Scherrer analysis of the XRD pattern, indicating a high crystallinity of the SnP NCs obtained. XRD characterization of the reaction product at different reaction times showed SnP to be directly produced from the reaction of the tin phosphonate complex and HMPT, with no intermediate phase forming (Figures S10 and S11). When excess TDPA (TDPA/Sn =2) was used, no solid was formed after 1 h of reaction with HMPT.

The complex collected after mixing tin oxalate with TDPA at 180 °C was a white viscous compound with very low solubility in any organic solvent tested. These characteristics were similar to those of the compound formed using a cadmium precursor. We thus hypothesize that the formed tin complex, most probably a tin tetradecylphoaphonate, is a coordination polymer similar to cadmium octadecylphosphonate, which was identified as composed of layers of cadmium ions bridged together by phosphonate groups.[9]

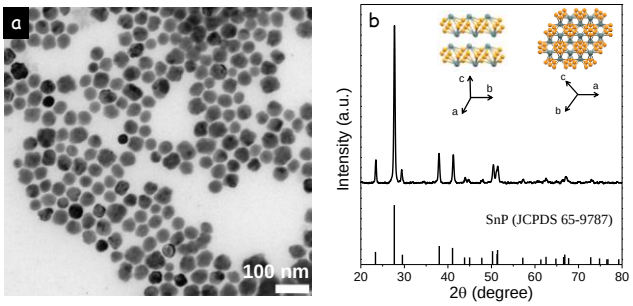

Figure 1. TEM micrograph (a) and XRD pattern (b) of the NCs produced from the reaction of tin oxalate with HMPT at 270 °C and in the presence of TDPA: TDPA/Sn = 1. Inset within the XRD graph shows the SnP crystal structure along two different directions.

Exchanging TDPA with a longer phosphonic acid, e.g. octadecylphosphonic acid (ODPA), maintaining otherwise identical conditions (ODPA/Sn =1, reaction temperature = 270 °C), resulted in smaller SnP NCs, with an average size of 23 ± 4 nm (Figures S7, S8). We ascribed this reduced NC size to a lower reactivity of the tin phosphonate complex formed from the longer chain phosphonic acid when compared with the shorter one, as also observed for cadmium chalcogenides.[10]

In agreement with XRD patterns, HRTEM analysis showed NCs to have the trigonal SnP crystallographic phase (S.G.: P-3ml) with lattice parameters a = b = 4.3922 Å and c = 6.0400 Å.[7] As described by J. Gullman, the SnP trigonal structure is formed by Sn octahedra filled with diphosphorous pairs that may have four different orientations (Figure S14).[7] In a perfect random distribution of the diphosphorous pairs orientations, no extra reflections should be observed in the power spectra (Figure S14e). However, the power spectrum of several NCs showed streaky extra spots as those observed in Figure S14b when visualizing the NC along the [10-10] zone axis. These streaky extra spots were in perfect agreement with the presence of stacking faults along the (0001) planes, i.e. in the sequence of the sandwiches composed of filled octahedral, as suggested by Y. Kim et al.[7-8] In other NCs, non-streaky extra spots were observed (red circles in figure 2c, see also S12-S16) which indicated the presence of an ordered superstructure as hypothetically suggested by J. Gullman in single crystals.[7] We attributed this superstructure to the ordered orientation of the diphosphorous pairs within the layers of filled octahedra. The structure model for a compound of the SnP type with the atomic pairs all oriented parallel with the c-axis was predicted by Hulliger,[11] but it was not previously experimentally reported.

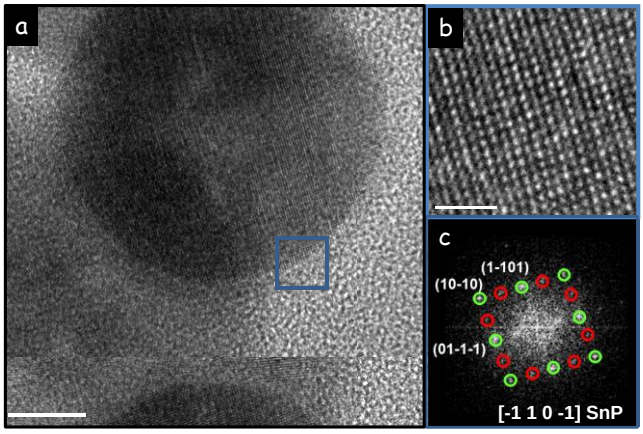

Figure 2 a) HRTEM micrograph of a SnP NC with the trigonal structure; b) Detail of the NC area squared in blue; and c) its corresponding power spectrum. In the power spectrum, besides the indexed spots (circled in green), some extra spots (circled in red), which should not exist in the pure hexagonal structure, were found.

Annular dark field scanning TEM (ADF-STEM) and STEM-EELS elemental composition maps revealed that Sn and P were uniformly distributed throughout each NC (Figure S17). SEM-EDS analysis showed that as-synthesized SnP NCs had an excess of phosphorous, P/Sn = 1.2 (Figure S6), which we attributed to the presence of phosphonate as surface ligand. The presence of a phosphonate surface ligand was further confirmed by FTIR and XPS analyses (Figure S18-S20).

EDX analysis of the NCs after ligand removal showed the phosphorous-to-tin ratio to be P/Sn = 0.96 ± 0.02. This phosphorous deficiency could be explained by considering a tin-rich surface after removal of the phosphate ligands. This deficiency was also consistent with J. Gullman[7] work, reporting SnP single crystals to have a significant amount of phosphorous vacancies and an overall stoichiometry: $SnP_{0.94}$.

For electrochemical measurements, SnP electrodes were prepared by mixing SnP NCs with carbon black (CB), carboxymethyl cellulose (CMC) and water, and casting the resulting slurries onto copper current collectors. Coin-type cells were employed for the electrochemical tests. The cell contained a sodium disk as counter and reference electrode, the SnP electrode as working electrode and a glass-fiber separator soaked with sodium electrolyte placed in-between both electrodes.

Figure 3a shows cyclic voltammetry curves of the SnP electrodes at a scan rate of 0.1 mV s^{-1}. In the first cathodic cycle (sodiation step), a small broad peak at about 0.5-0.9 V vs. Na^+/Na was attributed to the formation of a solid electrolyte interphase (SEI) layer due to irreversible reduction of the electrolyte during the first cycle.[12] Upon further sodiation, a large reduction peak at 0.07 V vs. Na^+/Na aroused, which was ascribed to sodium insertion in SnP to form $Na_{15}Sn_4$ and Na_3P phases.[3c]

In the reversed scan, the SnP electrode displayed two peaks at 0.46 V and 0.7 V, which can be associated with gradual desodiation of the $Na_{15}Sn_4$ phase.[13] In addition, the second peak at a higher potential, 0.7 V, can be assigned to desodiation of the Na_3P phase. Upon further cathodic cycles, three peaks at 0.57 V, 0.23 V and 0.01 V appeared. The peak at 0.57 V was attributed to the reaction of phosphorous with sodium,[14] and the peaks at 0.23 V and 0.01 V to the gradual sodiaton of Sn.

To identify the crystallographic phase evolution of the SnP electrode, in situ XRD analyses were performed (Figure S25). A steady decrease of the intensity of the SnP diffraction peaks and a concomitant peak broadening indicated that the sodiation of SnP NCs occurred with concomitant amorphization of the material. After desodiation, the SnP trigonal structure was not recovered and the material remained amorphous. Previous works using Sn_4P_3 particles observed a metallic tin segregation during cycling, which was related to the anode performance deterioration.[3b] In contrast, no phase segregation was observed during the sodiation and desodiation of SnP in the present work.

To maximize the battery performance, both the anode material and the liquid electrolyte need to be optimized. Electrolytes based on $NaClO_4$, $NaPF_6$ and sodium(I) bis(fluorosulfonyl)imide (NaFSI) salts were tested. Measuring the cycling performance of SnP anodes with the various sodium electrolytes, we concluded that the ultraconcentrated sodium electrolyte based on NaFSI in dimethoxyethane (DME) provided the highest stability (Figure S18). The enhanced electrochemical performance of SnP NCs with NaFSI electrolyte was attributed to the formation of a stable SEI that effectively suppress further electrolyte reduction during battery cycling.[12a, 15] NaFSI is actually the only electrolyte that, to a certain extent, can decrease sodium dendritic growth on Na metal during cycling.[12a] This advantage is related to its improved SEI stability. In addition, NaFSI electrolyte has a high oxidation stability and ionic conductivity.[12a]

Figure 3b shows rate-capability measurements of Na-ion half-cells based on SnP NCs at various current densities of 0.05 - 2.5 A g^{-1} yielding capacities of 645 - 396 mA h g^{-1}, respectively. Importantly, when the current rate was set back to 50 mA g^{-1} from the high current density of 2.5 A g^{-1}, almost full capacity recovery was measured. These results indicated a high electronic conductivity and charge-transfer kinetics in the SnP-based anode. As shown in the figure 3c, the voltage profiles during galvanostatic cycling were similar at all current densities. The galvanostatic curves were rather smooth, which suggest slow, gradual sodiation of SnP NCs.

The cycling stability tests of half-cells employing SnP NCs at current densities of 0.1 A g^{-1} and 0.5 A g^{-1} showed high capacity retention over 200 and 500 cycles (Figure 3d and S24) with high columbic efficiency of 98.3% and 99.0%. To the best of our knowledge, this is the longest cycle live demonstrated so far for tin phosphide-based anodes.[3b,c,f,g] We attribute the high electro-

chemical cyclic stability demonstrated for SnP NC-based electrodes to two factors: i) the small size of the particles, which prevents them from accumulating sufficient stresses to mechanically disintegrate during sodiation and desodiation cycles; and ii) to the convenient crystal structure and composition of the NCs, which maintained the SnP phase without segregation of tin and phosphorous during cycling.

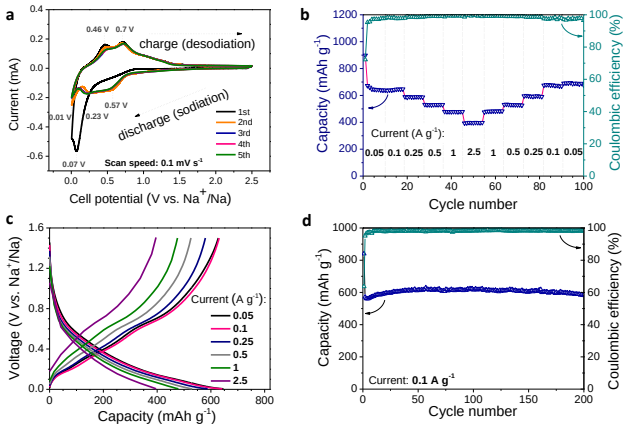

Figure 3. a) Cyclic voltammetry curves of the initial five charge-discharge cycles for electrodes comprising SnP NCs (scan rate = 0.1 mV s^{-1}) measured using 5M NaFSI in DME sodium electrolyte. b-d) Electrochemical performance of SnP NC-based anodes: b) Rate capability measurements, c) galvanostatic charge-discharge voltage curves; and d) cyclic stability of Na-ion half-cells employing SnP anodes made from SnP NCs at 0.1 A g^{-1}. All anodes had the same composition of SnP(64%)/CB(21%)/CMC(15%) and were cycled at room temperature at various current densities of 0.05 - 2.5 A g^{-1}; 5M NaFSI in DME solution was used as electrolyte for Na-ion cells. All batteries were cycled in the potential range of 5 mV - 1.5 V. The obtained capacities were normalized by the mass of SnP.

To summarize, pure-phase SnP NCs showing organized orientation of diphosphorous pairs within their layered crystal structure were produced. SnP NC-based SIB anodes exhibited specific capacity of about 600 mA h g^{-1} at a current density of 100 mA g^{-1} and very stable cycling performance with negligible capacity fading over 200 cycles. This excellent performance was attributed to the sodiation of the two components within the phosphide, the small size of the crystal domains and the proper phosphorous-rich composition.

ASSOCIATED CONTENT

Supporting Information.

The Supporting Information is available free of charge on the ACS Publications website.

Detailed experimental descriptions, material characterization and additional SIB test results

AUTHOR INFORMATION

Corresponding Author

* acabot@irec.cat

Funding Sources

No competing financial interests have been declared.

ACKNOWLEDGMENT

DN and JA acknowledge funding from Generalitat de Catalunya 2014 SGR 1638 and the Spanish MINECO coordinated projects between UJI, IREC and ICN2 VALPEC and ANAPHASE (ENE2017-85087-C3-3-R). ICN2 acknowledges support from the Severo Ochoa Programme (MINECO, Grant no. SEV-2013-0295) and is funded by the CERCA Programme / Generalitat de Catalunya. JL thanks the China Scholarship Council for scholarship support.

REFERENCES

(1) Luo, W.; Shen, F.; Bommier, C.; Zhu, H.; Ji, X.; Hu, L. *Acc. Chem. Res.* **2016**, 49, 231.

(2) (a) Qian, J.; Wu, X.; Cao, Y.; Ai, X.; Yang, H. *Angew. Chem. Int. Ed.* **2013**, 52, 4633. (b) Li, W.; Hu, S.; Luo, X.; Li, Z.; Sun, X.; Li, M.; Liu, F.; Yu, Y. *Adv. Mater.* **2017**, 29, 1605820.

(3) (a) Kim, Y.; Kim, Y.; Choi, A.; Woo, S.; Mok, D.; Choi, N. S.; Jung, Y. S.; Ryu, J. H.; Oh, S. M.; Lee, K. T. *Adv. Mater.* **2014**, 26, 4139. (b) Lan, D.; Wang, W.; shi, l.; Huang, Y.; Hu, L.; Li, Q. *J. Mater. Chem. A* **2017**, 5, 5791. (c) Qian, J.; Xiong, Y.; Cao, Y.; Ai, X.; Yang, H. *Nano lett.* **2014**, 14, 1865. (d) Li, Q.; Li, Z.; Zhang, Z.; Li, C.; Ma, J.; Wang, C.; Ge, X.; Dong, S.; Yin, L. *Adv. Energy Mater.* **2016**, 1600376. (e) Liu, J.; Kopold, P.; Wu, C.; van Aken, P. A.; Maier, J.; Yu, Y. *Energy Environ. Sci.* **2015**, 8, 3531. (f) Li, W.; Chou, S. L.; Wang, J. Z.; Kim, J. H.; Liu, H. K.; Dou, S. X. *Adv. Mater.* **2014**, 26, 4037. (g) Fan, X.; Mao, J.; Zhu, Y.; Luo, C.; Suo, L.; Gao, T.; Han, F.; Liou, S. C.; Wang, C. *Adv. Energy Mater.* **2015**, 5, 1500174. (h) Xu, Y.; Peng, B.; Mulder, F. M. *Adv. Energy Mater.* **2017**, 1701847. (i) Ma, L.; Yan, P.; Wu, S.; Zhu, G.; Shen, Y. *J. Mater. Chem. A* **2017**, 5, 16994.

(4) (a) Oszajca, M. F.; Bodnarchuk, M. I.; Kovalenko, M. V. *Chem. Mater.* **2014**, 26, 5422. (b) Wang, Q.; Zhao, C.; Lu, Y.; Li, Y.; Zheng, Y.; Qi, Y.; Rong, X.; Jiang, L.; Qi, X.; Shao, Y.; Pan, D.; Li, B.; Hu, Y. S.; Chen, L. *Small* **2017**, 13, 1701835.

(5) (a) Standing, A.; Assali, S.; Gao, L.; Verheijen, M. A.; van Dam, D.; Cui, Y.; Notten, P. H.; Haverkort, J. E.; Bakkers, E. P. *Nat. Commun.* **2015**, 6, 7824. (b) Sun, J.; Liu, C.; Yang, P. *J. Am. Chem. Soc.* **2011**, 133, 19306. (c) Tallapally, V.; Esteves, R. J. A.; Nahar, L.; Arachchige, I. U. *Chem.Mater.* **2016**, 28, 5406.

(6) Sushkova, T.P.; Kononova, E.U.; Savinova, Yu. A.; Dorokhina, E. S.; Semenova, G.V. *Condens. Matter. Inter.* **2014**, 16, 210.

(7) Gullman, J. *J. Solid State Chem.* **1990**, 87, 202.

(8) Kim, Y.; Hwang, H.; Yoon, C. S.; Kim, M. G.; Cho, J. *Adv. Mater.* **2007**, 19, 92.

(9) (a) Liu, H.; Owen, J. S.; Alivisatos, A. P. *J. Am. Chem. Soc.* **2007**, 129, 305. (b) Owen, J. S.; Park, J.; Trudeau, P. E.; Alivisatos, A. P. *J. Am. Chem. Soc.* **2008**, 130, 12279.

(10) Peng, Z. A.; Peng, X. *J. Am. Chem. Soc.* **2001**, 123, 1389.

(11) Hulliger, F. Structural chemistry of layer-type phases. Dordrecht, Holland, **1976**, pp. 145.

(12) (a) Lee, J.; Lee, Y.; Lee, J.; Lee, S. M.; Choi, J. H.; Kim, H.; Kwon, M. S.; Kang, K.; Lee, K. T.; Choi, N. S. *ACS Appl. Mater. Inter.* **2017**, 9, 3723. (b) Takada, K.; Yamada, Y.; Watanabe, E.; Wang, J.; Sodeyama, K.; Tateyama, Y.; Hirata, K.; Kawase, T.; Yamada, A. *ACS Appl. Mater. Inter.* **2017**, 9, 33802.

(13) Zheng, L.; Dunlap, R. A.; Obrovac, M. N. *J. Electro. Soc.* **2016**, 163, A1188.

(14) Dahbi, M.; Yabuuchi, N.; Fukunishi, M.; Kubota, K.; Chihara, K.; Tokiwa, K.; Yu, X. F.; Ushiyama, H.; Yamashita, K.; Son, J. Y.; Cui, Y. T.; Oji, H.; Komaba, S. *Chem. Mater.* **2016**, 28, 1625.

(15) Schafzahl, L.; Hanzu, L.; Wikening, M.; Freunberger, S. A. *ChemSusChem* **2017**, 10, 401.